

Performance Analysis of Multiband OFDM UWB Systems With Imperfect Synchronization and Intersymbol Interference

Hung-Quoc Lai, *Student Member, IEEE*, W. Pam Siritwongpairat, *Member, IEEE*, and K. J. Ray Liu, *Fellow, IEEE*

Abstract—This paper provides performance analysis of MB-OFDM UWB systems that not only captures the characteristics of realistic ultra-wideband (UWB) channels, but also takes into consideration of the imperfection of the frequency and timing synchronizations and the effect of intersymbol interference. The systems are considered in multipath fading channels, the IEEE 802.15.3a channel standard, with four channel models: CM1, CM2, CM3, and CM4. These channel models are characterized by cluster arrival rate, ray arrival rate within clusters, and cluster and ray decay factors. First, an average signal-to-noise ratio with imperfect synchronizations and intersymbol interference is derived. Then a closed-form bit error rate performance formulation that provides insightful understanding of the system performance in various synchronization conditions is obtained under Rayleigh fading assumption. This analytical performance formulation serves as an upper bound on the bit error rate performance of UWB systems. Finally, simulation results under various channel and synchronization conditions are provided to validate the theoretical analysis.

Index Terms—Bit-error rate, carrier-frequency offset, frequency synchronization, intercarrier interference, intersymbol interference, MB-OFDM, multipath fading channel, timing synchronization, ultra-wideband (UWB).

I. INTRODUCTION

IN April 2002, the U.S. Federal Communications Commission (FCC) published a report and order “Revision of Part 15 of the Commission Rules Regarding to Ultra-Wideband Transmission Systems” [1] that allows ultra-wideband (UWB) communication systems to be deployed on an unlicensed basis following Part 15 rules. The publication encourages researchers and engineers to devote their time and resources to the development of UWB transmission technology. According to the FCC’s definition, a UWB device is any device where the fractional bandwidth is greater than 20% of its center frequency or the minimum bandwidth is of 500 MHz. Besides, the FCC also defines the transmission power limits so that UWB devices are

allowed to coexist with other existing devices. Since the FCC’s publication, researchers and engineers have focused their attention to the frequency range from 3.1 to 10.6 GHz with the transmission power limit of -41.3 dBm/MHz, the highest transmission power allowance.

To exploit the unlicensed 7.5-GHz bandwidth, two technical approaches have mainly been proposed. The first approach is direct-sequence UWB (DS-UWB) relating to single-band systems. In this approach, binary phase-shift keying (BPSK) is employed to modulate the information into a sequence of UWB pulses [2]. The systems can operate in two different bands: the low band from 3.1 to 4.85 GHz and the high band from 6.2 to 9.7 GHz. The second approach involves multiband (MB) systems, and thus called MB-UWB. In this approach, the 7.5-GHz bandwidth is divided into subbands of more than 500 MHz each to comply with the FCC’s definition. The dominant candidate of this approach employs orthogonal frequency division multiplexing (OFDM) technique, the so-called MB-OFDM UWB [3].

MB-OFDM UWB systems support ten data rates from 53.3 to 480 Mbps [3] that are grouped into three data-rate modes, namely high-rate, middle-rate, and low-rate. These data-rate modes are classified using time-frequency coding (TFC) with overall spreading gain factors comprising from frequency spreading gain and time spreading gain. Three overall spreading gain factors of 1, 2, and 4 correspond to high-rate, middle-rate, and low-rate, respectively. Note that MB-OFDM UWB systems also use forward error correction (FEC) coding, together with the TFC, to distinguish the ten data rates. The FEC coding supports coding rates of 1/3, 11/32, 1/2, 5/8, and 3/4 obtained by puncturing the mother convolutional code with the rate of 1/3. In this paper, we do not address the system performance with the FEC coding.

The channel models specified in IEEE 802.15.3a channel standard [4] are based upon Saleh–Valenzuela (S–V) model [5], which is characterized by cluster arrival rate, ray arrival rate within clusters, and cluster and ray decay factors. The channel multipath gain coefficients are lognormal distributed. The performance of MB-OFDM UWB and DS-UWB systems was evaluated based on simulation in [6]. In [7], the authors analyzed the performance of MB-OFDM UWB systems under the imperfection of channel estimation. In [8], a general framework for the performance analysis of MB-OFDM UWB systems in IEEE 802.15.3a channel models was provided. All of the existing work assumed perfect frequency and timing synchronization. In addition, channel multipath delays were

Manuscript received December 1, 2006; revised July 15, 2007. This work was supported in part by the U.S. Army RDECOM CERDEC. The associate editor coordinating the review of this manuscript and approving it for publication was Prof. Dennis L. Goeckel.

H.-Q. Lai is with the U.S. Army RDECOM CERDEC, Fort Monmouth, NJ 07703 USA (e-mail: hungquoc.lai@us.army.mil).

W. P. Siritwongpairat is with the Meteor Communications Corporation, Kent, WA 98032 USA (e-mail: PSiritwongpairat@meteorcomm.com).

K. J. R. Liu is with the Department of Electrical and Computer Engineering and Institute for Systems Research, University of Maryland, College Park, MD 20742 USA (e-mail: kjrlu@eng.umd.edu).

Digital Object Identifier 10.1109/JSTSP.2007.906650

assumed to fit inside the cyclic prefix of OFDM symbols, and hence the systems would not suffer intersymbol interference (ISI). However in practice, multipath channel delays can exceed the length of OFDM cyclic prefix and cause ISI to the received signal in the systems. In addition, OFDM technique is sensitive to the imperfection of frequency and timing synchronizations.

This paper analyzes the performance of MB-OFDM UWB systems in realistic UWB channel models with the effect of both ISI and imperfect synchronization taken into consideration. Based on the channel models, we first derive an average signal-to-noise ratio (SNR) of the UWB systems under various synchronization conditions including perfect synchronization, imperfect timing synchronization, imperfect frequency synchronization, and imperfect frequency and timing synchronization. Then, we analyze the UWB system performance based on the average SNR. To simplify analysis and to get insights on the performance of UWB systems, we assume that the multipath gain coefficients have a statistically independent Gaussian distribution. Since typically, the UWB channel fading is lognormal fading which is less severe than the Rayleigh fading, the analysis under this Rayleigh fading assumption provides an upper bound on the bit-error rate (BER) performance of UWB systems. The analysis results in a closed-form average BER that provides an insightful understanding on the performance of the UWB system. Lastly, simulation results under various channel and synchronization conditions are provided to validate the theoretical analysis.

The content of this paper is outlined as follows. Channel and system models are presented in Section II. In Section III, the derivation of the average SNR is presented. The derivation of the average BER is presented in Section IV for the three data-rate modes. In Section V, we present and analyze the numerical and simulation results. Lastly, we draw several conclusions in Section VI.

II. CHANNEL AND SYSTEM MODELS

A. Channel Model

In this paper, the channel model is based on UWB standard channel models which are specified in IEEE 802.15.3a [4]. The UWB standard channel models are derived from S-V model [5] with some minor modifications due to clustering phenomenon. There are four UWB standard channel models, denoted as CM1, CM2, CM3, and CM4, which are based on the line-of-sight (LOS) multipath channel condition and the distance between the transmitter and the receiver. In general, the channel impulse response can be expressed as [4]

$$h(t) = \chi \sum_{l=0}^L \sum_{k=0}^K \alpha_{k,l} \delta(t - T_l - \tau_{k,l}) \quad (1)$$

where $\alpha_{k,l}$ are multipath gain coefficients, T_l is the delay of the l th cluster, $\tau_{k,l}$ is the delay of the k th ray in the l th cluster, $\delta(\cdot)$ is the Dirac's delta function, χ represents the log-normal shadowing, $(L + 1)$ is the number of arrival clusters, and $(K + 1)$ is the number of arrival rays within a cluster. For simplicity of the analysis, we will not consider χ in the expression of $h(t)$. In (1), cluster arrival times T_l 's and ray arrival times $\tau_{k,l}$'s within each cluster are modelled as time of arrivals in Poisson pro-

cesses with rate Λ and λ (where $\lambda > \Lambda$) [4], respectively. Thus, they are the l - and k -Erlang random variables with parameters Λ and λ , respectively. The standard UWB channel model is based on lognormal fading, in which multipath gain coefficients $\alpha_{k,l}$'s are modelled as statistically independent, zero-mean, lognormal random variables whose variance is [4]

$$\Omega_{k,l} = E \{ |\alpha_{k,l}|^2 | T_l, \tau_{k,l} \} = \Omega_{0,0} e^{-((T_l)/\Gamma) - ((\tau_{k,l})/\gamma)} \quad (2)$$

where Γ and γ are cluster and ray decay factors, respectively.

Note that $\tau_{0,l} = 0$ for all l , i.e., that the first ray in the l th cluster arrives when the cluster arrives [4]. In case of LOS condition (e.g., in CM1), the arrival time of the first cluster is $T_0 = 0$. Thus, (1) can be re-written for the case of LOS condition as [9]

$$h(t) = \alpha_{0,0} \delta(t) + \sum_{k=1}^K \alpha_{k,0} \delta(t - \tau_{k,0}) + \sum_{l=1}^L \alpha_{0,l} \delta(t - T_l) + \sum_{l=1}^L \sum_{k=1}^K \alpha_{k,l} \delta(t - T_l - \tau_{k,l}). \quad (3)$$

In case of non-LOS condition (e.g., in CM2, CM3, and CM4), all cluster arrival times T_l 's are random, and hence (1) can be re-expressed as

$$h(t) = \sum_{l=1}^L \alpha_{0,l} \delta(t - T_l) + \sum_{l=1}^L \sum_{k=1}^K \alpha_{k,l} \delta(t - T_l - \tau_{k,l}). \quad (4)$$

The channel model in (3) and (4) will be used in the subsequent performance analysis.

B. Signal Model

Fig. 1 illustrates the baseband model of MB-OFDM UWB systems. A data sequence $\{c_{0,i}, c_{1,i}, \dots, c_{n,i}, \dots, c_{N-1,i}\}$ with the OFDM symbol index i and the subcarrier index n ($n = 0, 1, \dots, N-1$) is input into the systems, where N is the number of subcarriers. The transmitted symbols $c_{n,i}$ are independent and identically distributed (i.i.d.) with the symbol energy E_s . Since two bits form a quadrature phase-shift keying (QPSK) symbol in the systems, $E_s = 2E_b$ where E_b is the bit energy. Transmitted OFDM symbols are generated using an N -point inverse discrete Fourier transform (IDFT). The useful OFDM symbols with a duration T_S are pre-appended by a cyclic prefix (actually zero-trailing) with a duration T_C to mitigate ISI and appended by a guard interval with a duration T_G to ensure a smooth transition between two consecutive OFDM symbols [3]. The output of the IDFT is

$$x_i(t) = \frac{1}{T_S} \sum_{n=0}^{N-1} c_{n,i} g(t - iT'_S) e^{((j2\pi n(t - iT'_S))/T_S)} \quad (5)$$

for $-\infty \leq i \leq \infty$

where $T'_S = T_C + T_S + T_G$ is the duration of the transmitted OFDM symbol, and

$$g(t) = \begin{cases} 1, & T_C \leq t \leq T_C + T_S \\ 0, & \text{otherwise} \end{cases} \quad (6)$$

is the rectangular pulse.

The transmitted signal $x(t) = \sum_{i=-\infty}^{\infty} x_i(t)$ travels through UWB channel. The received signal $r(t)$ is the sum of the channel

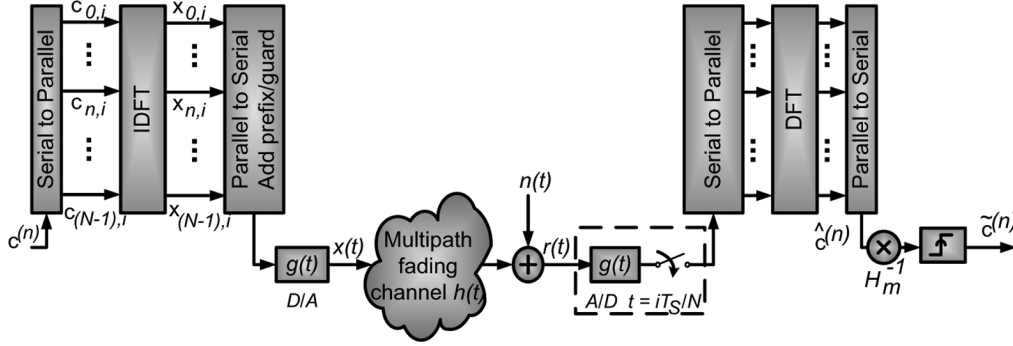


Fig. 1. System model.

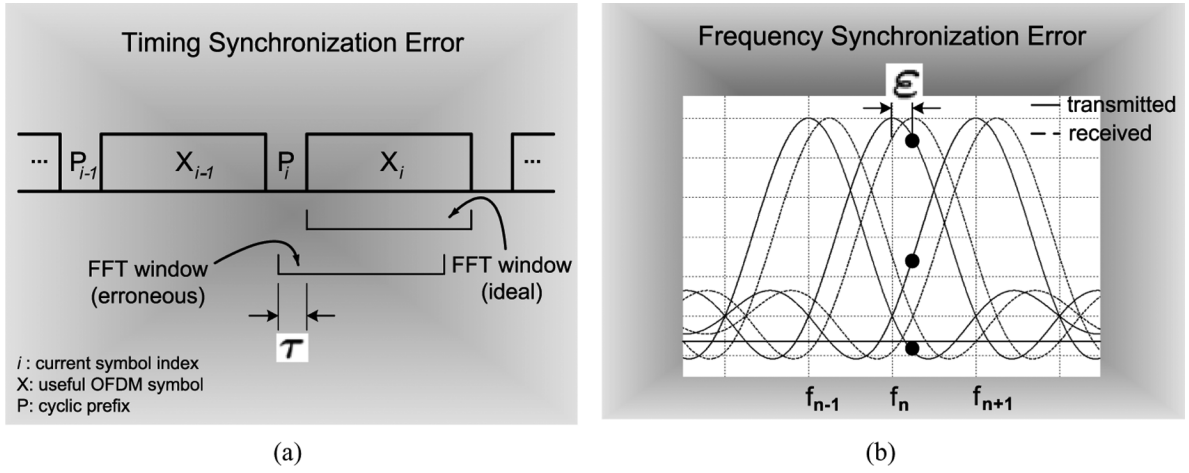


Fig. 2. (a) Timing synchronization error. (b) Frequency synchronization error.

output, $y(t)$, and the additive white Gaussian noise (AWGN), $v(t)$

$$r(t) = y(t) + v(t) = \sum_{i=-\infty}^{\infty} y_i(t) + v(t) \quad (7)$$

where

$$\begin{aligned} y_i(t) &= x_i(t) \star h(t) \\ &= \frac{1}{T_S} \sum_{n=0}^{N-1} c_{n,i} \sum_{l=0}^L \sum_{k=0}^K \alpha_{k,l} g(t - iT'_S - T_l - \tau_{k,l}) \\ &\quad \times e^{(j2\pi m(t - iT'_S - T_l - \tau_{k,l}))/T_S} \end{aligned} \quad (8)$$

is the channel output corresponding to OFDM symbol x_i , and (\star) denotes convolution. The channel, the transmitted symbols, and the AWGN are assumed mutually independent.

At the receiver, frequency and timing synchronization may not be perfect. The imperfection of frequency synchronization results in a carrier-frequency offset $\Delta f = f_r - f_t$ due to the mismatch between the oscillators of the transmitter and the receiver. Likewise, the error in timing synchronization causes timing offset τ due to misplacement of the discrete Fourier transform (DFT) window. Fig. 2 illustrates the imperfection of frequency and timing synchronizations. We assume that the cyclic prefix duration T_C is longer than the length of the timing error, i.e., $\tau \in (-T_C, T_C)$. Also, we assume that the multipath

delay is not longer than the symbol duration, i.e., $T_l + \tau_{k,l} \leq T_S$ for all k, l .

The demodulated signal in subcarrier m during the i th OFDM symbol period can be determined as

$$\hat{c}_{m,i} = \int_{iT'_S + T_C - \tau}^{iT'_S + T_C + T_S - \tau} r(t) e^{-j2\pi(f_{t,m} + \Delta f)(t - iT'_S)} dt \quad (9)$$

where $f_{t,m}$ is the transmitter carrier frequency corresponding to subcarrier m . Let $\epsilon = ((\Delta f)/(1/T_S)) = \Delta f T_S$ be the relative carrier-frequency offset. Substituting (7) into (9), we have

$$\begin{aligned} \hat{c}_{m,i} &= \int_{iT'_S + T_C}^{iT'_S + T_C + T_S} y_i(t - \tau) e^{((-j2\pi(m+\epsilon)(t - iT'_S - \tau))/T_S)} dt \\ &\quad + \sum_{i' \neq i} \int_{iT'_S + T_C}^{iT'_S + T_C + T_S} y_{i'}(t - \tau) \\ &\quad \times e^{((-j2\pi(m+\epsilon)(t - iT'_S - \tau))/T_S)} dt \\ &\quad + \int_{iT'_S + T_C}^{iT'_S + T_C + T_S} v(t) e^{((-j2\pi(m+\epsilon)(t - iT'_S - \tau))/T_S)} dt \\ &\triangleq A_{m,i} + \hat{c}_{m,i}^{ISI} + v_{m,i} \end{aligned} \quad (10)$$

where $A_{m,i}$ contains information related to the i th OFDM symbol, $\hat{c}_{m,i}^{ISI}$ results from the ISI from adjacent OFDM symbols, and $v_{m,i}$ is modelled as zero-mean complex Gaussian random variable with variance N_0 ($v_{m,i} \sim CN(0, N_0)$). Note that the average number of clusters arriving at the receiver at

a deterministic time T is $l_0 = \lfloor \Lambda T \rfloor$. For subsequent performance analysis, we assume all the rays within clusters T_l 's whose index $l \leq l_0$ arrive at the receiver before time T .

III. AVERAGE SIGNAL-TO-NOISE RATIO

In this section, we first derive the expressions of the fading term, the intercarrier interference (ICI) and the ISI, and then determine their variances. Based on the obtained variances, we analyze the UWB system performance in term of the degradation ratio.

A. Expressions of the Fading Term, the ICI, and the ISI

As shown in (10), the demodulated signal $\hat{c}_{m,i}$ comprises three components, including the signal information $A_{m,i}$, the ISI $\hat{c}_{m,i}^{ISI}$, and the additive noise $v_{m,i}$. These components are determined as follows.

From (10), we have

$$A_{m,i} = \int_{iT'_S+T_C}^{iT'_S+T_C+T_S} y_i(t-\tau) \times e^{((-j2\pi(m+\varepsilon)(t-iT'_S-\tau))/T_S)} dt. \quad (11)$$

Substituting $y_i(t)$ from (8) into (11) and applying the change of variable in t , we obtain

$$A_{m,i} = \frac{1}{T_S} \sum_{n=0}^{N-1} c_{n,i} \sum_{l=0}^L \sum_{k=0}^K \alpha_{k,l} \int_{T_C}^{T_C+T_S} g(t-X_{k,l}) \times w^{-n(t-X_{k,l})} w^{(m+\varepsilon)(t-\tau)} dt \quad (12)$$

where $X_{k,l} \triangleq T_l + \tau_{k,l} + \tau$ and $w \triangleq e^{((-j2\pi)/T_S)}$. Under the assumption that all the rays within clusters T_l 's for $l \leq l_0 = \lfloor \Lambda T \rfloor$, where T represents deterministic time, arrive at the receiver before T , $A_{m,i}$ in (12) can be expressed as

$$A_{m,i} = c_{m,i} H_m + \hat{c}_{m,i}^{ICI} \quad (13)$$

where

$$H_m = w^{\varepsilon T_C} w^{-(m+\varepsilon)\tau} \left[\sum_{l=0}^{l_0} \sum_{k=0}^K \alpha_{k,l} w^{mX_{k,l}} U_1 + \sum_{l=l_0+1}^L \sum_{k=0}^K \alpha_{k,l} w^{mX_{k,l}} U_2 \right] \quad (14)$$

contains the effect of fading (referred to as the fading term), and

$$\hat{c}_{m,i}^{ICI} = \sum_{n \neq m, n=0}^{N-1} c_{n,i} w^{-(n-m-\varepsilon)T_C} w^{-(m+\varepsilon)\tau} \times \left[\sum_{l=0}^{l_0} \sum_{k=0}^K \alpha_{k,l} U_3 + \sum_{l=l_0+1}^L \sum_{k=0}^K \alpha_{k,l} U_4 \right] \quad (15)$$

is the ICI from other subcarriers. In (14) and (15), $l_0 = \lfloor -\Lambda \tau \rfloor$. When $\tau > 0$, l_0 is negative. In such a case, l_0 in the second summation will take a value of zero. Also, in (14) and (15), U_1 , U_2 , U_3 and U_4 are defined as follows. In case that ε is not an integer,

$$U_1 = ((e^{-j2\pi\varepsilon} w^{\varepsilon X_{k,l}} - 1)/-j2\pi\varepsilon),$$

$$U_2 = ((e^{-j2\pi\varepsilon} - w^{\varepsilon X_{k,l}})/-j2\pi\varepsilon),$$

$$U_3 = ((e^{-j2\pi\varepsilon} w^{(m+\varepsilon)X_{k,l}} - w^{nX_{k,l}})/j2\pi(n-m-\varepsilon))$$

and

$$U_4 = ((e^{-j2\pi\varepsilon} w^{nX_{k,l}} - w^{(m+\varepsilon)X_{k,l}})/j2\pi(n-m-\varepsilon)).$$

In the case of $\varepsilon = 0$ (i.e., perfect synchronization), we have

$$U_1 = \lim_{\varepsilon \rightarrow 0} ((e^{-j2\pi\varepsilon} w^{\varepsilon X_{k,l}} - 1)/-j2\pi\varepsilon) = T_S + X_{k,l}$$

and

$$U_2 = \lim_{\varepsilon \rightarrow 0} ((e^{-j2\pi\varepsilon} - w^{\varepsilon X_{k,l}})/-j2\pi\varepsilon) = T_S - X_{k,l}.$$

In a case where ε is an integer (i.e., imperfect frequency synchronization with a multiple-subcarrier offset), we have

$$U_3 = \lim_{n \rightarrow (m+\varepsilon)} ((e^{-j2\pi\varepsilon} w^{(m+\varepsilon)X_{k,l}} - w^{nX_{k,l}})/j2\pi(n-m-\varepsilon))$$

$$= (1/T_S) w^{(m+\varepsilon)X_{k,l}} (T_S + X_{k,l})$$

and

$$U_4 = \lim_{n \rightarrow (m+\varepsilon)} ((e^{-j2\pi\varepsilon} w^{nX_{k,l}} - w^{(m+\varepsilon)X_{k,l}})/j2\pi(n-m-\varepsilon))$$

$$= (1/T_S) w^{(m+\varepsilon)X_{k,l}} (T_S - X_{k,l}).$$

Next, we determine the ISI component, $\hat{c}_{m,i}^{ISI}$, as follows. From (10)

$$\hat{c}_{m,i}^{ISI} = \sum_{i' \neq i} \int_{iT'_S+T_C}^{iT'_S+T_C+T_S} y_{i'}(t-\tau) \times e^{((-j2\pi(m+\varepsilon)(t-iT'_S-\tau))/T_S)} dt. \quad (16)$$

Under the assumptions that $\tau \in (-T_C, T_C)$ and $T_l + \tau_{k,l} \leq T_S$ for all k and l , only the previous $(i-1)$ th OFDM symbol involves in the current i th OFDM symbol. Therefore, (16) can be simplified to

$$\hat{c}_{m,i}^{ISI} = \int_{iT'_S+T_C}^{iT'_S+T_C+T_S} y_{i-1}(t-\tau) \times e^{((-j2\pi(m+\varepsilon)(t-iT'_S-\tau))/T_S)} dt. \quad (17)$$

Substituting $y_{i-1}(t)$ from (8) into (17), we obtain, after some manipulations

$$\hat{c}_{m,i}^{ISI} = \sum_{n=0}^{N-1} c_{n,i-1} w^{-(n-m-\varepsilon)T_C} \times w^{-(m+\varepsilon)\tau} \sum_{l=p_0+1}^L \sum_{k=0}^K \alpha_{k,l} U_5 \quad (18)$$

where

$$p_0 = \lfloor \Lambda(T_G + T_C - \tau) \rfloor$$

and

$$w = e^{(-j2\pi)/T_S}.$$

In (18),

$$U_5 = ((w^{(m+\varepsilon)(X_{k,l}-T_C-T_G)} - w^{n(X_{k,l}-T_C-T_G)})/j2\pi(n-m-\varepsilon))$$

when ε is not an integer, and

$$U_5 = \lim_{n \rightarrow (m+\varepsilon)} ((w^{(m+\varepsilon)(X_{k,l}-T_C-T_G)} - w^{n(X_{k,l}-T_C-T_G)})/j2\pi(n-m-\varepsilon)) = w^{(m+\varepsilon)(X_{k,l}-T_C-T_G)}(X_{k,l} - T_C - T_G) \text{ otherwise.}$$

B. Variances of the Fading Term, the ICI, and the ISI

Let us denote the variances of the fading term, the ICI, and the ISI as σ_H^2 , σ_C^2 , and σ_S^2 , respectively. Because the

$$\sigma_H^2 = \frac{1}{4\pi^2\varepsilon^2} \sum_{l=0}^{l_0} \sum_{k=0}^K E \left\{ \Omega_{0,0} e^{-(T_l/\Gamma) - (\tau_{k,l}/\gamma)} \left[2 - \left(e^{-j2\pi\varepsilon} w^{\varepsilon X_{k,l}} + e^{j2\pi\varepsilon} w^{-\varepsilon X_{k,l}} \right) \right] \right\} + \frac{1}{4\pi^2\varepsilon^2} \sum_{l=l_0+1}^L \sum_{k=0}^K E \left\{ \Omega_{0,0} e^{-(T_l/\Gamma) - (\tau_{k,l}/\gamma)} \left[2 - \left(e^{-j2\pi\varepsilon} w^{-\varepsilon X_{k,l}} + e^{j2\pi\varepsilon} w^{\varepsilon X_{k,l}} \right) \right] \right\} \quad (19)$$

$$\sigma_C^2 = E_s \sum_{n \neq m, n=0}^{N-1} \frac{1}{4\pi^2(n-m-\varepsilon)^2} \times \sum_{l=0}^{l_0} \sum_{k=0}^K E \left\{ \Omega_{0,0} e^{-(T_l/\Gamma) - (\tau_{k,l}/\gamma)} \left[2 - \left(e^{-j2\pi\varepsilon} w^{-(n-m-\varepsilon)X_{k,l}} + e^{j2\pi\varepsilon} w^{(n-m-\varepsilon)X_{k,l}} \right) \right] \right\} + E_s \sum_{n \neq m, n=0}^{N-1} \frac{1}{4\pi^2(n-m-\varepsilon)^2} \times \sum_{l=l_0+1}^L \sum_{k=0}^K E \left\{ \Omega_{0,0} e^{-(T_l/\Gamma) - (\tau_{k,l}/\gamma)} \left[2 - \left(e^{-j2\pi\varepsilon} w^{(n-m-\varepsilon)X_{k,l}} + e^{j2\pi\varepsilon} w^{-(n-m-\varepsilon)X_{k,l}} \right) \right] \right\} \quad (20)$$

$$\sigma_S^2 = E_s \sum_{n=0}^{N-1} \frac{1}{4\pi^2(n-m-\varepsilon)^2} \times \sum_{l=p_0+1}^L \sum_{k=0}^K E \left\{ \Omega_{0,0} e^{-(T_l/\Gamma) - (\tau_{k,l}/\gamma)} \left[2 - \left(w^{(n-m-\varepsilon)(X_{k,l}-T_C-T_G)} + w^{-(n-m-\varepsilon)(X_{k,l}-T_C-T_G)} \right) \right] \right\} \quad (21)$$

$$A_1 \triangleq \sum_{l=l_0+1}^{\infty} \sum_{k=1}^{\infty} E \left\{ \Omega_{0,0} e^{-(T_l/\Gamma) - (\tau_{k,l}/\gamma)} (T_l + \tau_{k,l} - T)^2 \right\} \quad (22)$$

$$A_2 \triangleq \sum_{p=p_0+1}^{\infty} E \left\{ \Omega_{0,0} e^{-((X_p)/\gamma_X)} (X_p - T)^2 \right\} \quad (23)$$

$$B_1 \triangleq \sum_{l=l_0+1}^{\infty} \sum_{k=1}^{\infty} E \left\{ \Omega_{0,0} e^{-(T_l/\Gamma) - (\tau_{k,l}/\gamma)} \times \left[2 - \left(e^{-j2\pi\varepsilon'} w^{(n-m-\varepsilon)(T_l+\tau_{k,l}-T)} + e^{j2\pi\varepsilon'} w^{-(n-m-\varepsilon)(T_l+\tau_{k,l}-T)} \right) \right] \right\} \quad (24)$$

$$B_2 \triangleq \sum_{p=p_0+1}^{\infty} E \left\{ \Omega_{0,0} e^{-((X_p)/\gamma_X)} \left[2 - \left(e^{-j2\pi\varepsilon'} w^{(n-m-\varepsilon)(X_p-T)} + e^{j2\pi\varepsilon'} w^{-(n-m-\varepsilon)(X_p-T)} \right) \right] \right\} \quad (25)$$

transmitted symbols $c_{n,i}$'s and the multipath gain coefficients $\alpha_{k,l}$'s are zero-mean, H_m , $\hat{c}_{m,i}^{\text{ICI}}$, and $\hat{c}_{m,i}^{\text{ISI}}$ are also zero-mean. Thus, $\sigma_H^2 = E\{|H_m|^2\}$, $\sigma_C^2 = E\{|\hat{c}_{m,i}^{\text{ICI}}|^2\}$, and $\sigma_S^2 = E\{|\hat{c}_{m,i}^{\text{ISI}}|^2\}$. From the expressions of H_m , $\hat{c}_{m,i}^{\text{ICI}}$, and $\hat{c}_{m,i}^{\text{ISI}}$ derived in the previous section, their variances can be determined as shown in (19)–(21), at the bottom of the previous page. For notational convenience, we introduce the quantities shown in (22)–(25), also shown at the bottom of the previous page, where $E\{\cdot\}$ denotes expectation and $w = e^{(-j2\pi)/T_S}$ as defined in Section III-A. In these equations, T_l , $\tau_{k,l}$, and X_p are arrival times in Poisson processes whose rates are Λ , λ , and λ_X and the decay factors are Γ , γ , and γ_X , respectively. Based on (3), the variances of interest will be separated in terms of A_1 , A_2 , B_1 , and B_2 with different values of T , n , m , ε , ε' , λ_X , and γ_X . Notice that T_l , $\tau_{k,l}$, and X_p are l -, k -, and p -Erlang random variables. The derivation of these quantities are omitted; the results are given as shown in (26)–(29), at the bottom of the page, where we have (30)–(34), also shown at the bottom of the page.

Now the variances σ_H^2 , σ_C^2 and σ_S^2 can be derived in terms of A_1 , A_2 , B_1 , and B_2 . To simplify the presentation, we summarize below the results in case of LOS channels and $\tau < 0$:

- 1) Perfect frequency and timing synchronization, i.e., $\varepsilon = 0$ and $\tau = 0$:

$$\sigma_H^2 = \Omega_{0,0} + \frac{1}{T_S^2} A_2(T_S, 0, \lambda, \gamma) + \frac{1}{T_S^2} A_2(T_S, 0, \Lambda, \Gamma) + \frac{1}{T_S^2} A_1(T_S, 0, \Lambda, \Gamma, \lambda, \gamma) \quad (35)$$

$$\sigma_C^2 = E_s \sum_{n \neq m, n=0}^{N-1} \frac{1}{4\pi^2(n-m)^2} \times \left[B_2(0, n, m, 0, 0, 0, \lambda, \gamma) + B_2(0, n, m, 0, 0, 0, \Lambda, \Gamma) + B_1(0, n, m, 0, 0, 0, \Lambda, \Gamma, \lambda, \gamma) \right] \quad (36)$$

$$\sigma_S^2 = E_s \left[\frac{1}{T_S^2} A_2(T_C + T_G, p_0, \Lambda, \Gamma) + \frac{1}{T_S^2} A_1(T_C + T_G, p_0) + \sum_{n \neq m, n=0}^{N-1} \frac{1}{4\pi^2(n-m)^2} \times \left[B_2(T_C + T_G, n, m, 0, 0, p_0, \Lambda, \Gamma) + B_1(T_C + T_G, n, m, 0, 0, p_0, \Lambda, \Gamma, \lambda, \gamma) \right] \right] \quad (37)$$

$$A_1 = \Omega_{0,0} \left[\Gamma^2 f_3(l_0, \Lambda, \Gamma) f_1(0, \lambda, \gamma) + \gamma^2 f_1(l_0, \Lambda, \Gamma) f_3(0, \lambda, \gamma) + T^2 f_1(l_0, \Lambda, \Gamma) f_1(0, \lambda, \gamma) + 2\Gamma\gamma f_2(l_0, \Lambda, \Gamma) f_2(0, \lambda, \gamma) - 2T\Gamma f_2(l_0, \Lambda, \Gamma) f_1(0, \lambda, \gamma) - 2T\gamma f_1(l_0, \Lambda, \Gamma) f_2(0, \lambda, \gamma) \right] \quad (26)$$

$$A_2 = \Omega_{0,0} \left[\gamma_X^2 f_3(p_0, \lambda_X, \gamma_X) + T^2 f_1(p_0, \lambda_X, \gamma_X) - 2T\gamma_X f_2(p_0, \lambda_X, \gamma_X) \right] \quad (27)$$

$$B_1 = 2\Omega_{0,0} f_1(l_0, \Lambda, \Gamma) f_1(0, \lambda, \gamma) - 2\Omega_{0,0} \beta_T^{l_0+1} \beta_\tau \times \left[\frac{\cos\left((l_0+1)\theta_T + \theta_\tau - \frac{2\pi(n-m-\varepsilon)T}{T_S} + 2\pi\varepsilon'\right) - \beta_\tau \cos\left((l_0+1)\theta_T - \frac{2\pi(n-m-\varepsilon)T}{T_S} + 2\pi\varepsilon'\right)}{(1 + \beta_T^2 - 2\beta_T \cos \theta_T)(1 + \beta_\tau^2 - 2\beta_\tau \cos \theta_\tau)} - \frac{\beta_T \cos\left(l_0\theta_T + \theta_\tau - \frac{2\pi(n-m-\varepsilon)T}{T_S} + 2\pi\varepsilon'\right) + \beta_T \beta_\tau \cos\left(l_0\theta_T - \frac{2\pi(n-m-\varepsilon)T}{T_S} + 2\pi\varepsilon'\right)}{(1 + \beta_T^2 - 2\beta_T \cos \theta_T)(1 + \beta_\tau^2 - 2\beta_\tau \cos \theta_\tau)} \right] \quad (28)$$

$$B_2 = 2\Omega_{0,0} f_1(p_0, \lambda_X, \gamma_X) - 2\Omega_{0,0} \beta_X^{p_0+1} \times \left[\frac{\cos\left((p_0+1)\theta_X - \frac{2\pi(n-m-\varepsilon)T}{T_S} + 2\pi\varepsilon'\right) - \beta_X \cos\left(p_0\theta_X - \frac{2\pi(n-m-\varepsilon)T}{T_S} + 2\pi\varepsilon'\right)}{1 + \beta_X^2 - 2\beta_X \cos \theta_X} \right] \quad (29)$$

$$f_1(p, a, b) \triangleq \frac{(ab)^{p+1}(ab+1)}{(ab+1)^{p+1}} \quad (30)$$

$$f_2(p, a, b) \triangleq \frac{(ab)^{p+1}(ab+p+1)}{(ab+1)^{p+1}} \quad (31)$$

$$f_3(p, a, b) \triangleq \frac{(ab)^{p+1} [2ab(ab+1) + 2(p+1)ab + (p+1)(p+2)]}{(ab+1)^{p+2}} \quad (32)$$

$$\beta_X \triangleq \frac{\lambda_X}{\sqrt{\left(\lambda_X + \frac{1}{\gamma_X}\right)^2 + \frac{4\pi^2(n-m-\varepsilon)^2}{T_S^2}}} \quad (33)$$

$$\theta_X \triangleq \arctan\left(\frac{2\pi(n-m-\varepsilon)}{T_S} \frac{\gamma_X}{\lambda_X \gamma_X + 1}\right) \quad (34)$$

2) Imperfect timing synchronization, i.e., $\varepsilon = \mathbf{0}$ and $\tau \neq \mathbf{0}$: see (38)–(40), as shown at the bottom of the page.

3) Imperfect frequency synchronization, i.e., $\varepsilon \neq \mathbf{0}$ and $\tau = \mathbf{0}$:

$$\sigma_H^2 = \frac{1}{4\pi^2\varepsilon^2} \left[2\Omega_{0,0}(1 - \cos 2\pi\varepsilon) + B_2(0,0,0,\varepsilon,\varepsilon,0,\lambda,\gamma) + B_2(0,0,0,\varepsilon,\varepsilon,0,\Lambda,\Gamma) + B_1(0,0,0,\varepsilon,\varepsilon,0,\Lambda,\Gamma,\lambda,\gamma) \right] \quad (41)$$

$$\sigma_C^2 = E_s \sum_{n \neq m, n=0}^{N-1} \frac{1}{4\pi^2(n-m-\varepsilon)^2} \times \left[2\Omega_{0,0}(1 - \cos 2\pi\varepsilon) + B_2(0,n,m,\varepsilon,\varepsilon,0,\lambda,\gamma) + B_2(0,n,m,\varepsilon,\varepsilon,0,\Lambda,\Gamma) + B_1(0,n,m,\varepsilon,\varepsilon,0,\Lambda,\Gamma,\lambda,\gamma) \right] \quad (42)$$

$$\sigma_S^2 = E_s \sum_{n=0}^{N-1} \frac{1}{4\pi^2(n-m-\varepsilon)^2} \times \left[B_2(T_C + T_G, n, m, \varepsilon, 0, p_0, \Lambda, \Gamma) + B_1(T_C + T_G, n, m, \varepsilon, 0, p_0, \Lambda, \Gamma, \lambda, \gamma) \right] \quad (43)$$

4) Imperfect frequency and timing synchronization, i.e., $\varepsilon \neq \mathbf{0}$ and $\tau \neq \mathbf{0}$: see (44)–46, at the bottom of the next page. where $l_0 = \lfloor -\Lambda\tau \rfloor$ and $p_0 = \lfloor \Lambda(T_G + T_C - \tau) \rfloor$. Note that the variances in cases of non-LOS or $\tau \geq 0$ can be simply obtained in a similar way.

C. Average Signal-to-Noise Ratio

In the previous subsection, the variances of the fading term, the ICI and the ISI are obtained. Beside the fading and the interferences, the received symbol is also affected by AWGN $v_{m,i}$ whose variance is N_0 . Thus the average SNR per QPSK symbol can be defined as

$$\bar{\gamma}_s(\varepsilon, \tau) \triangleq \frac{E_s \sigma_H^2}{\sigma_C^2 + \sigma_S^2 + N_0}. \quad (47)$$

Since the energy per bit $E_b = (1/2)E_s$, the average SNR per bit $\bar{\gamma}_b(\varepsilon, \tau) = (1/2)\bar{\gamma}_s(\varepsilon, \tau)$.

IV. AVERAGE BIT ERROR RATE

Average BER, which measures the absolute performance, is defined as a ratio of the number of bits incorrectly received to the total number of bits sent. To simplify analysis and to get insights on the UWB system performance, we assume in the following analysis that the multipath gain coefficients $\alpha_{k,l}$'s have a statistically independent Gaussian distribution with zero mean and variances $\Omega_{k,l}$. Since typically, the UWB channel fading is lognormal fading which is less severe than the Rayleigh fading,

$$\sigma_H^2 = \Omega_{0,0} \frac{(\tau + T_S)^2}{T_S^2} + \frac{1}{T_S^2} A_2(-T_S - \tau, 0, \lambda, \gamma) + \frac{1}{T_S^2} A_2(-T_S - \tau, 0, \Lambda, \Gamma) - \frac{1}{T_S^2} A_2(-T_S - \tau, l_0, \Lambda, \Gamma) + \frac{1}{T_S^2} A_2(T_S - \tau, l_0, \Lambda, \Gamma) + \frac{1}{T_S^2} A_1(-T_S - \tau, 0, \Lambda, \Gamma, \lambda, \gamma) - \frac{1}{T_S^2} A_1(-T_S - \tau, l_0, \Lambda, \Gamma, \lambda, \gamma) + \frac{1}{T_S^2} A_1(T_S - \tau, l_0, \Lambda, \Gamma, \lambda, \gamma) \quad (38)$$

$$\sigma_C^2 = E_s \sum_{n \neq m, n=0}^{N-1} \frac{1}{4\pi^2(n-m)^2} \times \left[2\Omega_{0,0} \left(1 - \cos \frac{2\pi(n-m)\tau}{T_S} \right) + B_2(-\tau, n, m, 0, 0, 0, \lambda, \gamma) + B_2(-\tau, n, m, 0, 0, 0, \Lambda, \Gamma) + B_1(-\tau, n, m, 0, 0, 0, \Lambda, \Gamma, \lambda, \gamma) \right] \quad (39)$$

$$\sigma_S^2 = E_s \left[\frac{1}{T_S^2} A_2(T_C + T_G - \tau, p_0, \Lambda, \Gamma) + \frac{1}{T_S^2} A_1(T_C + T_G - \tau, p_0, \Lambda, \Gamma, \lambda, \gamma) + \sum_{n \neq m, n=0}^{N-1} \frac{1}{4\pi^2(n-m)^2} \times \left[B_2(T_C + T_G - \tau, n, m, 0, 0, p_0, \Lambda, \Gamma) + B_1(T_C + T_G - \tau, n, m, 0, 0, p_0, \Lambda, \Gamma, \lambda, \gamma) \right] \right] \quad (40)$$

the analysis under this Rayleigh fading assumption provides an upper bound on the BER performance of UWB systems.

According to (10) and (13), the demodulated signal $\hat{c}_{m,i}$ at the m th subcarrier can be expressed as

$$\hat{c}_{m,i} = c_{m,i}H_m + z_m \quad (48)$$

where $z_m \triangleq \hat{c}_{m,i}^{\text{ICI}} + \hat{c}_{m,i}^{\text{ISI}} + v_{m,i}$ represents the summation of the ICI, the ISI and the AWGN. In Section III-A, we have seen that $\hat{c}_{m,i}^{\text{ICI}}$ and $\hat{c}_{m,i}^{\text{ISI}}$ are the sums of independent random variables. The ICI and the ISI have zero mean and variances σ_C^2 and σ_S^2 , respectively. To obtain the performance bound, we model the ICI and the ISI as Gaussian random variables [10]. This can be done because independent Gaussian noise yields smallest capacity among additive noise processes with fixed variance and mean [11]. Consequently, z_m will be modelled as i.i.d. complex Gaussian random variables whose mean is zero and variance is $\sigma_Z^2 = \sigma_C^2 + \sigma_S^2 + N_0$.

The UWB systems support ten data rates [3] that can be grouped into three data-rate modes based on overall spreading gain factors of 1, 2, or 4. These three cases share the same receiving model, i.e.,

$$\hat{\mathbf{c}} = c_{m,i}\mathbf{h} + \mathbf{z} \quad (49)$$

where $\hat{\mathbf{c}}$ is a vector comprising demodulated signals $\hat{c}_{m,i}$, \mathbf{h} is a vector consisting of fading terms H_m associated with $\hat{c}_{m,i}$, and

$\mathbf{z} \sim CN(0, \sigma_Z^2 \mathbb{I})$, with identical matrix \mathbb{I} , is the noise vector. Depending on the data-rate modes, $\hat{\mathbf{c}}$, \mathbf{h} , and \mathbf{z} are different and will be classified later. To detect the information symbols, the receiver can incorporate equalization and perform optimal sequential detection, or it can use a suboptimal detector. In what follows, we assume that the information symbol is detected according to the decision rule:

$$\tilde{c}_{m,i} = \underset{c_{m,i}}{\text{argmin}} \|\hat{\mathbf{c}} - c_{m,i}\mathbf{h}\|^2. \quad (50)$$

Since the system employs QPSK modulation, the average BER, denoted as P_b , is determined through the average symbol error rate P_s as $P_b = P_s/2$, where P_s is determined by averaging symbol error rate given random vector \mathbf{h} , i.e., $P_s = E\{P_s(\mathbf{h})\}$. Based on the detection rule, we have [13]

$$P_s(\mathbf{h}) = Q\left(\sqrt{2\rho}\right) \quad (51)$$

where $Q(\cdot)$ represents the well-known Q -function, defined as $Q(x) = \int_x^\infty \frac{1}{\sqrt{2\pi}} \exp(-t^2/2) dt$ [14]. In (51), ρ is defined as

$$\rho = \|\mathbf{h}\|^2 \frac{E_b}{\sigma_Z^2} \quad (52)$$

using the fact that the distance between QPSK symbols $|c_{m,i} - \tilde{c}_{m,i}|$ relates to the energy per bit E_b as $|c_{m,i} - \tilde{c}_{m,i}| = 2\sqrt{E_b}$.

$$\sigma_H^2 = \frac{1}{4\pi^2\varepsilon^2} \left[2\Omega_{0,0} \left(1 - \cos\left(\frac{2\pi\varepsilon\tau}{T_S} + 2\pi\varepsilon\right) \right) + B_2(-\tau, 0, 0, \varepsilon, -\varepsilon, 0, \lambda, \gamma) \right. \\ \left. + B_2(-\tau, 0, 0, \varepsilon, -\varepsilon, 0, \Lambda, \Gamma) - B_2(-\tau, 0, 0, \varepsilon, -\varepsilon, l_0, \Lambda, \Gamma) \right. \\ \left. + B_2(-\tau, 0, 0, \varepsilon, \varepsilon, l_0, \Lambda, \Gamma) + B_1(-\tau, 0, 0, \varepsilon, -\varepsilon, 0, \Lambda, \Gamma, \lambda, \gamma) \right. \\ \left. - B_1(-\tau, 0, 0, \varepsilon, -\varepsilon, l_0, \Lambda, \Gamma, \lambda, \gamma) + B_1(-\tau, 0, 0, \varepsilon, \varepsilon, l_0, \Lambda, \Gamma, \lambda, \gamma) \right] \quad (44)$$

$$\sigma_C^2 = E_s \sum_{n \neq m, n=0}^{N-1} \frac{1}{4\pi^2(n-m-\varepsilon)^2} \\ \times \left[2\Omega_{0,0} \left(1 - \cos\left(\frac{2\pi(n-m-\varepsilon)\tau}{T_S} - 2\pi\varepsilon\right) \right) \right. \\ \left. + B_2(-\tau, n, m, \varepsilon, -\varepsilon, 0, \lambda, \gamma) + B_2(-\tau, n, m, \varepsilon, -\varepsilon, 0, \Lambda, \Gamma) \right. \\ \left. - B_2(-\tau, n, m, \varepsilon, -\varepsilon, l_0, \Lambda, \Gamma) + B_2(-\tau, n, m, \varepsilon, \varepsilon, l_0, \Lambda, \Gamma) \right. \\ \left. + B_1(-\tau, n, m, \varepsilon, -\varepsilon, 0, \Lambda, \Gamma, \lambda, \gamma) - B_1(-\tau, n, m, \varepsilon, -\varepsilon, l_0, \Lambda, \Gamma, \lambda, \gamma) \right. \\ \left. + B_1(-\tau, n, m, \varepsilon, \varepsilon, l_0, \Lambda, \Gamma, \lambda, \gamma) \right] \quad (45)$$

$$\sigma_S^2 = E_s \sum_{n=0}^{N-1} \frac{1}{4\pi^2(n-m-\varepsilon)^2} \\ \times \left[B_2(T_C + T_G - \tau, n, m, \varepsilon, 0, p_0, \Lambda, \Gamma) \right. \\ \left. + B_1(T_C + T_G - \tau, n, m, \varepsilon, 0, p_0, \Lambda, \Gamma, \lambda, \gamma) \right] \quad (46)$$

Our remaining task is to determine the probability density function (PDF) $f_\rho(t)$ of the random variable ρ for the three data-rate modes. The average symbol error rate then is given by [12], [13]

$$P_s = \int_0^\infty f_\rho(t) Q(\sqrt{2t}) dt. \quad (53)$$

Note that when ρ is a chi-square random variable with $2d$ degrees of freedom, its PDF is [12]

$$f_\rho(t) = \frac{1}{(d-1)!(\overline{\gamma}_\rho)^d} t^{d-1} e^{-t/\overline{\gamma}_\rho} \text{ for } t \geq 0 \quad (54)$$

where $\overline{\gamma}_\rho \triangleq E\{\rho\}$ is the expectation of ρ corresponding to $d = 1$. Thus the average symbol error rate is [12]

$$P_s = p^d \sum_{k=0}^{d-1} \binom{d-1+k}{k} (1-p)^k \quad (55)$$

where

$$p \triangleq \frac{1}{2} \left(1 - \sqrt{\frac{\overline{\gamma}_\rho}{1+\overline{\gamma}_\rho}} \right). \quad (56)$$

Note that the proposed MB-OFDM UWB standard also uses FEC codes with coding rates of 1/3, 11/32, 1/2, 5/8, and 3/4 in conjunction with the TFC. Performance analysis of the FEC coded system can be obtained as follows. First, we determine the average BER of an uncoded system. Then, we can determine the performance bound of the FEC coded system based on the obtained average BER and the FEC information such as free distances and weight spectrum [13]. The detailed analysis on the FEC coded system is not included in this paper due to the space limitation.

In the following, we will demonstrate that ρ is approximately chi-square distributed with $2d$ degrees of freedom where d is the overall spreading gain factor.

A. When Overall Spreading Gain Factor is 1

In this case, each frequency carrier and each time slot are used to transmit different information. The quantities in (49) are $\hat{\mathbf{c}} = \hat{c}_{m,i}$, $\mathbf{h} = H_m$, and $\mathbf{z} = z$. Thus $\rho = ((E_b)/\sigma_Z^2) |H_m|^2$. From (14), we can rewrite the fading term as

$$H_m = \frac{1}{-j2\pi\varepsilon} w^{\varepsilon T_C} w^{-(m+\varepsilon)\tau} \mathbf{w}^H \mathbb{T} \mathbf{a} \quad (57)$$

where

$$\mathbf{w} = \left[w^{m(T_0+\tau_0,0+\tau)}, w^{m(T_0+\tau_0,1+\tau)}, \dots, w^{m(T_L+\tau_{K,L}+\tau)} \right]^T,$$

$$\mathbb{T} = \text{diag} \left(e^{-j2\pi\varepsilon w^{\varepsilon(T_0+\tau_0,0+\tau)}} - 1, \dots, e^{-j2\pi\varepsilon w^{\varepsilon(T_0+\tau_{K,0}+\tau)}} - 1, \dots, e^{-j2\pi\varepsilon w^{\varepsilon(T_{l_0+1}+\tau_0, l_0+1+\tau)}} - 1, \dots, e^{-j2\pi\varepsilon w^{\varepsilon(T_L+\tau_{K,L}+\tau)}} - 1 \right)$$

and

$$\mathbf{a} = [\alpha_{0,0}, \alpha_{0,1}, \dots, \alpha_{K,L}]^T.$$

Because $\alpha_{k,l} \sim CN(0, \Omega_{k,l})$ where $\Omega_{k,l}$ follows (2), we have $\mathbf{a} = \mathbf{\Omega}^{(1/2)} \mathbf{b}$ where $\mathbf{\Omega}^{(1/2)} \mathbf{\Omega}^{(1/2)} = \mathbf{\Omega} =$

$\text{diag}(\Omega_{0,0}, \Omega_{0,1}, \dots, \Omega_{K,L})$ and $\mathbf{b} = [\beta'_{0,0}, \beta'_{0,1}, \dots, \beta'_{K,L}]^T$, where $\beta'_{k,l} \sim CN(0, 1)$. Therefore

$$H_m = \frac{1}{-j2\pi\varepsilon} w^{\varepsilon T_C} w^{-(m+\varepsilon)\tau} \mathbf{w}^H \mathbb{T} \mathbf{\Omega}^{(1/2)} \mathbf{b} \quad (58)$$

and consequently

$$\rho = \frac{E_b}{\sigma_Z^2} \frac{1}{4\pi^2\varepsilon^2} \mathbf{b}^H \mathbf{\Omega}^{(1/2)} \mathbb{T} \mathbf{w} \mathbf{w}^H \mathbb{T} \mathbf{\Omega}^{(1/2)} \mathbf{b}. \quad (59)$$

Let us define $\mathbf{\Psi} = \mathbf{\Omega}^{(1/2)} \mathbb{T} \mathbf{w} \mathbf{w}^H \mathbb{T} \mathbf{\Omega}^{(1/2)}$. Clearly, $\mathbf{\Psi}$ is a non-negative definite Hermitian matrix. Based on the singular-value decomposition theorem [15], we can express $\mathbf{\Psi} = \mathbf{V} \mathbf{\Lambda} \mathbf{V}^H$ where $\mathbf{\Lambda}$ is a diagonal matrix containing the real and non-negative eigenvalues of $\mathbf{\Psi}$ and \mathbf{V} is a unitary matrix containing the eigenvectors associating with the eigenvalues in $\mathbf{\Lambda}$. Since $\text{rank}(\mathbf{\Psi}) \leq \min\{\text{rank}(\mathbf{\Omega}^{(1/2)}), \text{rank}(\mathbb{T}), \text{rank}(\mathbf{w})\}$ where $\text{rank}(\mathbf{\Omega}^{(1/2)}) = \text{rank}(\mathbb{T}) = (K+1)(L+1)$ and $\text{rank}(\mathbf{w}) = 1$, there exists in $\mathbf{\Lambda}$ only one nonzero eigenvalue, which can be evaluated as

$$\begin{aligned} \text{eig}(\mathbf{\Psi}) &= \sum_{l=0}^{l_0} \sum_{k=0}^K \Omega_{k,l} [2 - (e^{-j2\pi\varepsilon w^{\varepsilon X_{k,l}}} + e^{j2\pi\varepsilon w^{-\varepsilon X_{k,l}}})] \\ &+ \sum_{l=l_0+1}^L \sum_{k=0}^K \Omega_{k,l} [2 - (e^{-j2\pi\varepsilon w^{-\varepsilon X_{k,l}}} + e^{j2\pi\varepsilon w^{\varepsilon X_{k,l}}})]. \end{aligned}$$

Thus, substituting $\Omega_{k,l}$ from (2), we have

$$\begin{aligned} \rho &= \frac{E_b}{\sigma_Z^2} \frac{1}{4\pi^2\varepsilon^2} \\ &\times \left(\sum_{l=0}^{l_0} \sum_{k=0}^K \Omega_{0,0} e^{-(T_l/\Gamma) - (\tau_{k,l}/\gamma)} \right. \\ &\quad \times [2 - (e^{-j2\pi\varepsilon w^{\varepsilon X_{k,l}}} + e^{j2\pi\varepsilon w^{-\varepsilon X_{k,l}}})] \\ &\quad + \sum_{l=l_0+1}^L \sum_{k=0}^K \Omega_{0,0} e^{-(T_l/\Gamma) - (\tau_{k,l}/\gamma)} \\ &\quad \left. \times [2 - (e^{-j2\pi\varepsilon w^{-\varepsilon X_{k,l}}} + e^{j2\pi\varepsilon w^{\varepsilon X_{k,l}}})] \right) |\beta|^2 \quad (60) \end{aligned}$$

where $\beta \sim CN(0, 1)$.

Equation (60) reveals that ρ is not a chi-square random variable with two degrees of freedom as in the case of the Rayleigh fading channel [12], [13]. Here, ρ is a product of a chi-square random variable $|\beta|^2$ and another random variable that is the sum of many combinations of the k - and l - Erlang random variables T_l and $\tau_{k,l}$. Hence, finding the PDF of ρ is difficult, if not impossible.

To obtain a closed-form formulation of the BER performance, we employ the approximation approach in [8] as follows. From (52), ρ has a quadratic form. Using a representation of quadratic form in [16], and noting that $E\{\mathbf{h}\} = 0$, we get

$$\rho \approx \frac{E_b}{\sigma_Z^2} \sum_{s=1}^S \text{eig}_s(\mathbf{\Phi}) |\mu_s|^2 \quad (61)$$

where $\mu_s \sim CN(0, 1)$ and S is the rank of matrix $\mathbf{\Phi}$, defined as $\mathbf{\Phi} \triangleq E\{\mathbf{h}\mathbf{h}^H\}$. For the case of the gain factor of 1, $\mathbf{h} =$

H_m , thus $\Phi = \sigma_H^2$, which is the variance of the fading term. Consequently

$$\rho \approx \frac{E_b \sigma_H^2}{\sigma_Z^2} |\mu|^2. \quad (62)$$

Since $\mu \sim CN(0, 1)$, $|\mu|^2$ has a chi-square probability distribution with two degrees of freedom. Hence ρ approximately is chi-square distributed with two degrees of freedom. Equation (62) also reveals that the expectation of ρ is $\bar{\gamma}_\rho = \bar{\gamma}_b(\varepsilon, \tau)$, the average SNR per bit.

Based on (55) with $d = 1$ and (56), the average symbol error rate and hence the average BER for this case is

$$P_b = P_s \approx \frac{1}{2} \left(1 - \sqrt{\frac{\bar{\gamma}_b(\varepsilon, \tau)}{1 + \bar{\gamma}_b(\varepsilon, \tau)}} \right). \quad (63)$$

B. When Overall Spreading Gain Factor is 2

In this case, the same information is transmitted in two consecutive time slots. In such a case, (49) has $\hat{\mathbf{c}} = [\hat{c}_{m,i} \ \hat{c}_{m,i+1}]^T$, $\mathbf{h} = [H_m \ H_m]^T$, and $\mathbf{z} \sim CN(0, \sigma_Z^2 \mathbb{I}_2)$, assuming that the fading terms at the same subcarrier index m are i.i.d. Following the same procedures as in Section IV-A, we can show that

$$\begin{aligned} \rho &= \frac{E_b}{\sigma_Z^2} \frac{1}{4\pi^2 \varepsilon^2} \\ &\times \left(\sum_{l=0}^{l_0} \sum_{k=0}^K \Omega_{0,0} e^{-(T_l/\Gamma) - (\tau_{k,l}/\gamma)} \right. \\ &\quad \times [2 - (e^{-j2\pi\varepsilon} w^{\varepsilon X_{k,l}} + e^{j2\pi\varepsilon} w^{-\varepsilon X_{k,l}})] \\ &\quad + \sum_{l=l_0+1}^L \sum_{k=0}^K \Omega_{0,0} e^{-(T_l/\Gamma) - (\tau_{k,l}/\gamma)} \\ &\quad \times [2 - (e^{-j2\pi\varepsilon} w^{-\varepsilon X_{k,l}} + e^{j2\pi\varepsilon} w^{\varepsilon X_{k,l}})] \left. \right) \\ &\times (|\beta_1|^2 + |\beta_2|^2) \end{aligned} \quad (64)$$

where $\beta_i \sim CN(0, 1)$, $i = 1, 2$. The result in (64) reveals that in this case ρ relates to a chi-square random variable with four degrees of freedom.

Observe that the matrix

$$\Phi \triangleq E \{ \mathbf{h} \mathbf{h}^H \} = \begin{pmatrix} \sigma_H^2 & 0 \\ 0 & \sigma_H^2 \end{pmatrix} \quad (65)$$

has two eigenvalues $\text{eig}_1(\Phi) = \text{eig}_2(\Phi) = \sigma_H^2$. Hence, similar to Section IV-A, ρ can be approximated as

$$\rho \approx \frac{E_b \sigma_H^2}{\sigma_Z^2} (|\mu_1|^2 + |\mu_2|^2) \quad (66)$$

where $\mu_i \sim CN(0, 1)$, $i = 1, 2$. Therefore, the average symbol error rate and hence the average BER for the case of $d = 2$ can be approximated as

$$P_b = P_s \approx p^2(3 - 2p) \quad (67)$$

where p is defined in (56) with $\bar{\gamma}_\rho = \bar{\gamma}_b(\varepsilon, \tau)$.

C. When Overall Spreading Gain Factor is 4

In this case, the same information is transmitted four times using two frequency carriers and two consecutive time slots. Accordingly, (49) has

$$\begin{aligned} \hat{\mathbf{c}} &= [\hat{c}_{m,i} \ \hat{c}_{m,i+1} \ \hat{c}_{N-m-1,i}^* \ \hat{c}_{N-m-1,i+1}^*]^T \\ \mathbf{h} &= [H_m \ H_m \ H_{N-m-1}^* \ H_{N-m-1}^*]^T, \end{aligned}$$

and $\mathbf{z} \sim CN(0, \sigma_Z^2 \mathbb{I}_4)$. Following the same procedures as in Section IV-A, we have

$$\begin{aligned} \rho &= \frac{E_b}{\sigma_Z^2} \frac{1}{4\pi^2 \varepsilon^2} \\ &\times \left(\sum_{l=0}^{l_0} \sum_{k=0}^K \Omega_{0,0} e^{-(T_l/\Gamma) - (\tau_{k,l}/\gamma)} \right. \\ &\quad \times [2 - (e^{-j2\pi\varepsilon} w^{\varepsilon X_{k,l}} + e^{j2\pi\varepsilon} w^{-\varepsilon X_{k,l}})] \\ &\quad + \sum_{l=l_0+1}^L \sum_{k=0}^K \Omega_{0,0} e^{-(T_l/\Gamma) - (\tau_{k,l}/\gamma)} \\ &\quad \times [2 - (e^{-j2\pi\varepsilon} w^{-\varepsilon X_{k,l}} + e^{j2\pi\varepsilon} w^{\varepsilon X_{k,l}})] \left. \right) \\ &\times (|\beta_1|^2 + |\beta_2|^2 + |\beta_3|^2 + |\beta_4|^2) \end{aligned} \quad (68)$$

where $\beta_i \sim CN(0, 1)$, $i = 1, 2, 3, 4$, and the matrix

$$\Phi \triangleq E \{ \mathbf{h} \mathbf{h}^H \} = \begin{pmatrix} \sigma_H^2 & 0 & R & R \\ 0 & \sigma_H^2 & R & R \\ R^* & R^* & \sigma_H^2 & 0 \\ R^* & R^* & 0 & \sigma_H^2 \end{pmatrix}$$

where $R = E \{ H_m H_{N-m-1} \}$ is the complementary correlation between the fading terms at subcarrier m and its symmetric conjugate at subcarrier $N - m - 1$. From H_m in (14), we can show that we have (69), as shown at the bottom of the page, where Γ' and γ' are defined

$$\begin{aligned} R &= \frac{1}{4\pi^2 \varepsilon^2} w^{(N-1)\tau} \sum_{l=0}^{l_0} \sum_{k=0}^K E \left\{ \Omega_{0,0} e^{-((T_l)/\Gamma') - ((\tau_{k,l})/\gamma')} [2 - (e^{-j2\pi\varepsilon} w^{\varepsilon X_{k,l}} + e^{j2\pi\varepsilon} w^{-\varepsilon X_{k,l}})] \right\} \\ &\quad + \frac{1}{4\pi^2 \varepsilon^2} w^{(N-1)\tau} \sum_{l=l_0+1}^L \sum_{k=0}^K E \left\{ \Omega_{0,0} e^{-((T_l)/\Gamma') - ((\tau_{k,l})/\gamma')} [2 - (e^{-j2\pi\varepsilon} w^{-\varepsilon X_{k,l}} + e^{j2\pi\varepsilon} w^{\varepsilon X_{k,l}})] \right\} \\ &\triangleq R(N-1) \end{aligned} \quad (69)$$

such that $((1)/\Gamma') = ((1)/\Gamma) + ((j2\pi(N-1))/T_S)$ and $((1)/\gamma') = ((1)/\gamma) + ((j2\pi(N-1))/T_S)$. By replacing Γ and γ in (19) with Γ' and γ' , respectively, and multiplying the equation by $w^{(N-1)\tau}$, we obtain $R(N-1)$ in (69).

Let us define $r \triangleq ((R(N-1))/\sigma_H^2)$ as the normalized complementary correlation. Then the eigenvalues of matrix Φ can be shown as $\text{eig}(\Phi) = \sigma_H^2[1 + |r|, 1, 1, 1 - |r|]^T$. Consequently

$$\rho \approx \frac{E_b \sigma_H^2}{\sigma_Z^2} ((1 + |r|)|\mu_1|^2 + |\mu_2|^2 + |\mu_3|^2 + (1 - |r|)|\mu_4|^2) \quad (70)$$

where $\mu_i \sim CN(0, 1)$, $i = 1, 2, 3, 4$. Based on (70), the average symbol error rate can be determined in the two specific cases as follows.

- 1) When $|r| \ll 1$, r can be ignored in (70). Hence, ρ approximately is a chi-square random variable with eight degrees of freedom. Thus from (55) with $d = 4$, the average symbol error rate, and hence the average BER in this case is

$$P_b = P_s \approx p^4 \sum_{k=0}^3 \binom{3+k}{k} (1-p)^k \quad (71)$$

where p is defined in (56) with $\overline{\gamma}_\rho = \overline{\gamma}_b(\varepsilon, \tau)$.

- 2) When r cannot be ignored, ρ is no longer chi-square distributed because it is not a sum of i.i.d. random variables. This reflects the fact that the fading in different subchannels are highly correlated to each other. To find the average symbol error rate, we use the alternative representation of the Q -function [17], $Q(x) = (1/\pi) \int_0^{\pi/2} \exp(-(x^2)/2 \sin^2 \theta) d\theta$ for $x \geq 0$. The average symbol error rate can then be expressed as

$$P_s = \frac{1}{\pi} \int_0^{\pi/2} M_\rho \left(-\frac{1}{\sin^2 \theta} \right) d\theta \quad (72)$$

where $M_\rho(s) = E\{e^{s\rho}\}$ is the moment generating function of ρ . Because ρ is the sum of independent chi-square random variables, it can be shown that

$$M_\rho(s) \approx \frac{1}{(1 - s\overline{\gamma}_\rho(1 + |r|))(1 - s\overline{\gamma}_\rho)^2(1 - s\overline{\gamma}_\rho(1 - |r|))} \quad (73)$$

where $\overline{\gamma}_\rho = \overline{\gamma}_b(\varepsilon, \tau)$.

For MB-OFDM UWB systems, (71) and (72) yield similar results since the normalized complementary correlation r is relatively small. For example, in the case of perfect frequency and timing synchronization, r equals 0.0987, 0.0141, 0.0018, and 7.8343×10^{-4} , computed for CM1, CM2, CM3, and CM4, respectively. Fig. 3 shows the average BER for the perfect synchronization case in CM1, CM2, CM3, and CM4. The average BER is plotted using (71) in the dotted-diamond curve (denoted as Approximate) and (72) in the solid curve (denoted as Exact). Clearly, the approximated BER closely matches the exact BER.

We have completely derived the average BER for MB-OFDM UWB systems. For the case of high-rate and middle-rate mode, the average BER follows (63) and (67), respectively. The average BER for the low-rate mode takes the form of (71) or (72), depending on the value of the normalized complementary correlation r .

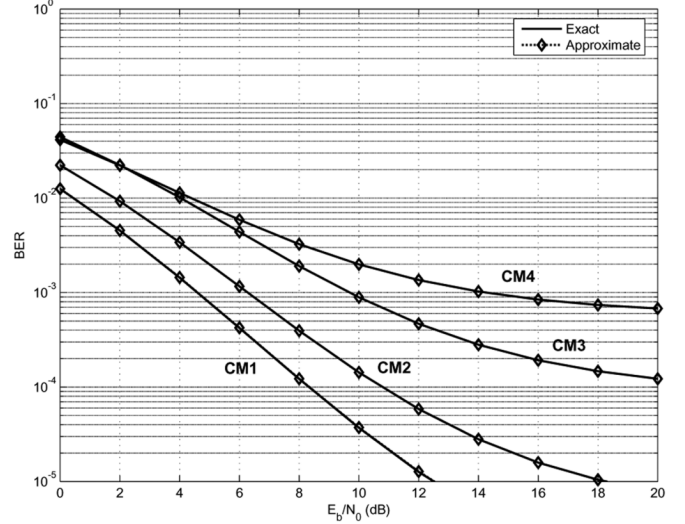


Fig. 3. Average BER of MB-OFDM UWB systems for low-rate mode—with and without r .

V. NUMERICAL AND SIMULATION RESULTS

Performance of MB-OFDM UWB systems is considered in UWB channel models with various conditions of frequency and timing synchronizations. The OFDM system has $N = 128$ subcarriers with the subband bandwidth of 528 MHz. The durations of the useful OFDM symbol, the cyclic prefix, and the guard interval are $T_S = 242.42$ nsec, $T_C = 60.61$ nsec, and $T_G = 9.47$ nsec, respectively. The arrival rates Λ and λ and the decay factors Γ and γ of the cluster and ray, respectively, follow [4].

In Section V-A, the numerical results will be presented and analyzed. For the purpose of demonstration, the numerical results are obtained in the two extreme channels: CM1 and CM4. The low-rate mode is chosen for the clarity of the demonstration. The simulation results will be presented in Section V-B.

A. Numerical Results

The first figure of interest is Fig. 4, which illustrates the UWB system performance in the perfect frequency and timing synchronization. The figure shows the system performance in the three data-rate modes. The following observations are from the figure. First, as the data rate increases, at the same SNR, the average BER also increases. This is caused by the spreading gain the data-rate mode inherits. The higher the spreading gain factor is the more diversity order, and hence the lower the average BER. Secondly, the average BER increases as the severity of the channel increases. This is obvious in the figure. CM1 is the least severe channel with the lowest average BER while CM4 is the most severe channel with the highest average BER, when compared at the same SNR and the same data-rate mode. Lastly, the figure reveals the ISI effect on the system performance with the error floors that can be observed at high SNR. The ISI effect is embedded in the generated channel when the channel multipath delays exceed the cyclic-prefix duration.

Fig. 5 illustrates the UWB system performance in the imperfect timing synchronization. The performance is obtained in the low-rate mode with various timing errors where

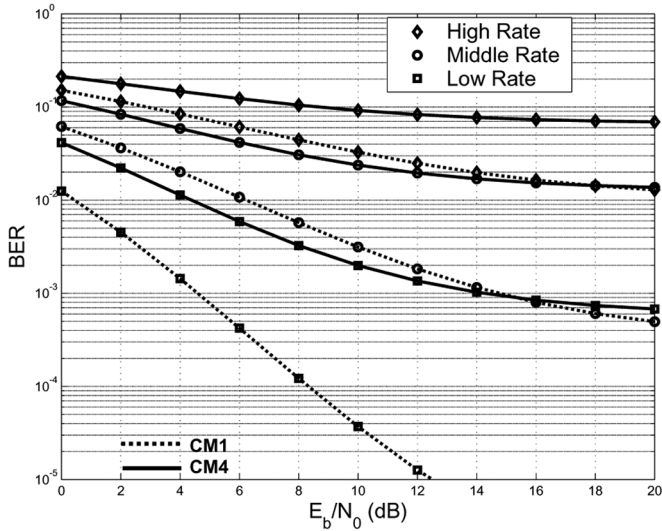


Fig. 4. Average BER of MB-OFDM UWB systems in perfect frequency and timing synchronization.

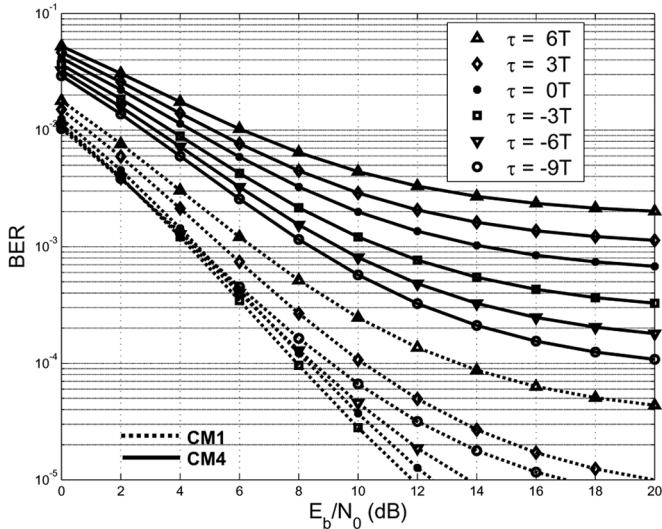


Fig. 5. Average BER of MB-OFDM UWB systems for low-rate mode in imperfect timing synchronization.

$T = ((T_S)/128)$. From the figure, positive timing errors always worsen the system performance. As illustrated in Fig. 2(a), positive timing errors correspond to misplacement of the FFT window toward the previous OFDM symbol. This causes the current OFDM symbol to pick up more signals from the previous OFDM symbol, resulting higher ISI and worse performance. Fig. 5 also shows that small negative timing errors yield better system performance; however, large negative timing errors degrade the system performance a great deal. As illustrated in Fig. 2(a), negative timing errors correspond to misplacement of the FFT window away from the previous OFDM symbol. This helps reducing the delay effect of arriving signals from the previous OFDM symbol, resulting a better performance in case of small negative timing errors when the information is detected based on the decision rule in (50). However, for large negative timing errors, the loss of the first several rays in the first cluster of the arriving signals of the current OFDM symbol causes the

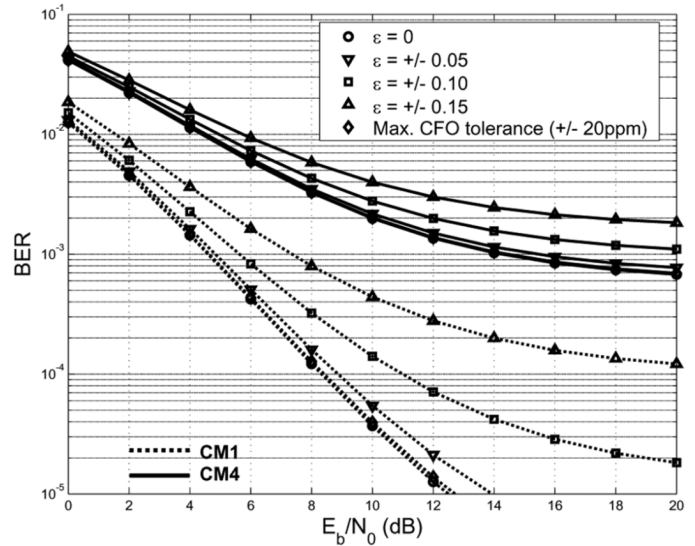


Fig. 6. Average BER of MB-OFDM UWB systems for low-rate mode in imperfect frequency synchronization.

degradation of the system performance. Note that these major rays possess a relatively large energy in the arriving signals since the cluster and ray amplitudes decay exponentially. Here, we see a trade-off between the delay of arriving signals from the previous OFDM symbol that causes the ISI and the loss of major rays in the arriving signals from the current OFDM symbol. Lastly, more severe channel tolerates more timing synchronization errors. Note that the more severe the channel is the larger the delay. Such channel allows larger negative timing errors since negative timing errors tend to reduce the channel delays.

The UWB system performance in the imperfect frequency synchronization is described by Fig. 6, where the performance is obtained in the low-rate mode with various relative carrier-frequency offsets. Note that negative and positive frequency errors with the same magnitude yield the same performance. Two observations are from the figure. First, as the ϵ magnitude increases, the system performance becomes worse. As illustrated in Fig. 2(b), the demodulated signal $\hat{c}_{m,i}$ in term of energy, contains less the desired symbol $c_{m,i}$ due to smaller H_m magnitude while contains more other symbols (the undesired ones). As a result, frequency synchronization errors increase the ICI and degrade the system performance. Secondly, similarly to the case of imperfect timing synchronization, more severe channel tolerates more frequency synchronization errors. In Fig. 6, the distance between two consecutive curves in CM1 is larger than that of CM4. Since the performance is relatively bad in the severe channels due to ISI, the same amount of carrier-frequency offset causes a relatively small degradation to the system performance. Fig. 6 also shows the system performance at the maximum carrier frequency offset (CFO) tolerance of ± 20 ppm, as specified in [3]. Since there are 14 bands in the proposed standard, the tolerance in the figure is computed for Band 2 with center frequency of 3960 MHz for the demonstration purpose, and it is equivalent to $\epsilon = 0.02$. The figure reveals that the UWB system performance in the maximum CFO tolerance is about the same with that in the perfect frequency synchronization (i.e., $\epsilon = 0$).

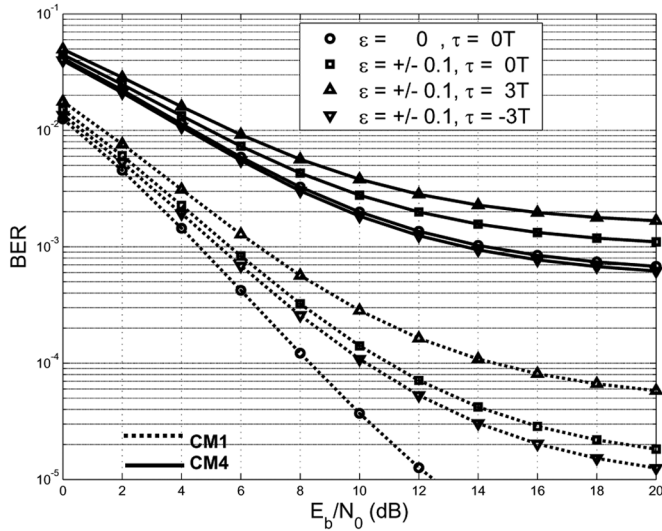


Fig. 7. Average BER of MB-OFDM UWB systems for low-rate mode in imperfect frequency and timing synchronization.

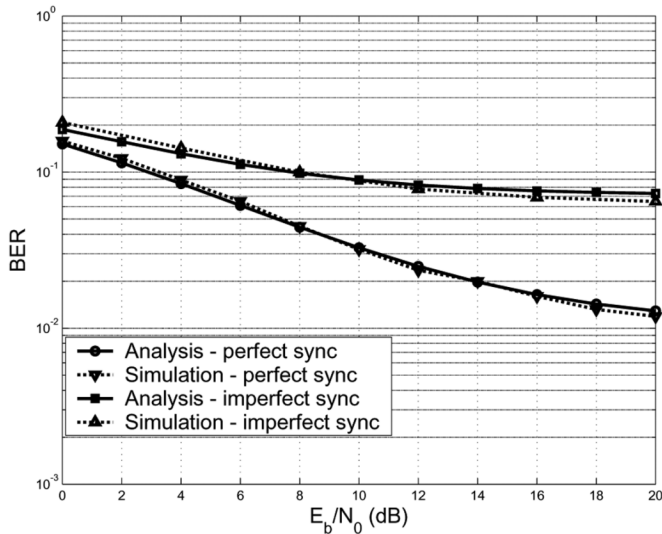


Fig. 8. Average BER of MB-OFDM UWB systems for high-rate mode in channel model CM1: simulation versus analysis.

The last figure of interest is Fig. 7, which illustrates the combined effect from frequency and timing synchronization errors on the system performance. As mentioned above, negative and positive frequency synchronization errors have the same degradation effect to the system performance. On the other hand, positive timing errors cause more performance degradation than the negative timing errors.

B. Simulation versus Numerical Results

Fig. 8 presents simulation results versus numerical results of the UWB system performance. For demonstration purposes, two cases are presented: perfect and imperfect synchronization in CM1 with the high-rate mode. These two cases correspond to $\varepsilon = 0, \tau = 0$ and $\varepsilon = 0.2, \tau = 3T$, respectively. We can see the simulation curves match the numerical curves very well. In case of middle-rate and low-rate modes, transmit information is jointly encoded across time and frequency, and we expect

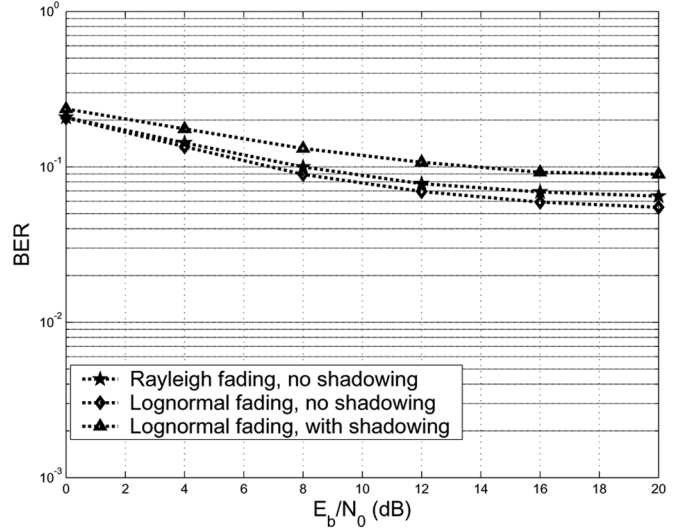


Fig. 9. Average BER of MB-OFDM UWB systems for high-rate mode in channel model CM1: Rayleigh fading versus lognormal fading—simulation results.

the same performance match and thus omit the simulation. The simulation results validate the theoretical analysis.

Since UWB channel standard suggests the use of lognormal fading and lognormal shadowing for the UWB channel model, Fig. 9 compares simulated performance under various fading scenarios, including Rayleigh fading without shadowing, lognormal fading without shadowing, and lognormal fading with shadowing. The case under the simulation corresponds to imperfect synchronization with $\varepsilon = 0.2$ and $\tau = 3T$ in CM1 with high-rate mode. The results confirm our expectation that, in case of no shadowing, the performance under lognormal fading channel is a bit better than that under Rayleigh fading channel. Also, the performance under channels with both fading and shadowing is worse than that under pure fading channel, as expected. For example, without shadowing, the performance under lognormal fading channel is about 1dB better than that under Rayleigh fading channel at BER of 10^{-1} . With the shadowing effect taken into account, the performance degrades by about 5 dB at the BER of 10^{-1} .

VI. CONCLUSIONS

We provide performance analysis of MB-OFDM UWB systems in the four IEEE 802.15.3a channel models under four conditions of frequency and timing synchronizations. We first derive the average SNR of the systems in the standard channel models. Then we analyze the system performance in terms of average BER. The analysis provides us an insightful understanding of the system performance in the standard channel models under different conditions of the frequency and timing synchronizations. A number of numerical results provides a visual observation of the UWB system performance in various synchronization conditions. Simulations are presented for the validation of the theoretical analysis. In addition, simulations provide a comparison of system performance in channels of Rayleigh fading without shadowing, lognormal fading without shadowing, and lognormal fading with lognormal shadowing.

REFERENCES

- [1] Revision of Part 15 of the Commission's Rules Regarding Ultra Wideband Transmission Systems, First Report and Order [Online]. Available: http://www.fcc.gov/Bureaus/Engineering_Technology/Orders/2002/fcc02048.pdf
- [2] R. Fisher *et al.*, DS-UWB Physical Layer Submission to 802.15 Task Group 3a 2004, Tech. Rep., IEEE 802.15-04/0137r00137r00137r0.
- [3] A. Batra *et al.*, Multi-Band OFDM Physical Layer Proposal for IEEE 802.15 Task Group 3a 2004, Tech. Rep., IEEE 802.15-03/268r3.
- [4] J. Foerster *et al.*, Channel Modeling Sub-Committee Report Final 2004, Tech. Rep., IEEE 802.15-02/368r5-SG3a.
- [5] A. Saleh and R. Valenzuela, "A statistical model for indoor multipath propagation," *IEEE J. Select. Areas Commun.*, vol. SAC-5, no. 1, pp. 128–137, Feb. 1987.
- [6] O. Shin, S. Ghassemzadeh, L. Greenstein, and V. Tarokh, "Performance evaluation of MB-OFDM and DS-UWB systems for wireless personal area networks," in *Proc. IEEE ICUBW'05*, Sep. 2005, pp. 214–219.
- [7] C. Snow, L. Lampe, and R. Schober, "Performance analysis of multi-band OFDM for UWB communication," in *Proc. IEEE ICC'05*, May 2005, vol. 4, pp. 2573–2578.
- [8] W. P. Siritwongpairat, W. Su, and K. J. R. Liu, "Performance characterization of multiband UWB communication systems using Poisson cluster arriving fading paths," *IEEE J. Select. Areas Commun.*, vol. 24, no. 4, pp. 745–751, Apr. 2006.
- [9] H. Q. Lai, W. Siritwongpairat, and K. J. R. Liu, "Performance analysis of MB-OFDM UWB system with imperfect synchronization and intersymbol interference," in *Proc. IEEE ICASSP'07*, Apr. 2006, vol. 3, pp. III-569–III-572.
- [10] Y. H. Kim, I. Song, H. G. Kim, T. Chang, and H. M. Kim, "Performance analysis of a coded OFDM system in time-varying multipath Rayleigh fading channels," *IEEE Trans. Veh. Technol.*, vol. 48, no. 5, pp. 1610–1615, Sep. 1999.
- [11] T. M. Cover and J. A. Thomas, *Elements of Information Theory*. New York: Wiley, 1991.
- [12] J. R. Barry, E. A. Lee, and D. G. Messerschmitt, *Digital Communication*, 3rd ed. Norwell, MA: Kluwer, 2004.
- [13] J. G. Proakis, *Digital Communications*, 4th ed. New York: McGraw-Hill, 2001.
- [14] A. Leon-Garcia, *Probability and Random Processes for Electrical Engineering*, 2nd ed. Reading, MA: Addison-Wesley-Longman, 1994.
- [15] R. A. Horn and C. R. Johnson, *Matrix Analysis*. New York: Cambridge Univ. Press, 1985.
- [16] A. M. Mathai and S. B. Provost, *Quadratic Forms in Random Variables: Theory and Applications*. New York: Marcel Dekker, 1992.
- [17] M. K. Simon and M. S. Alouini, *Digital Communication over Fading Channels: A Unified Approach to Performance Analysis*. New York: Wiley, 2000.



Hung-Quoc Lai (S'03) received the B.S. (cum laude) and M.S. degrees in electrical engineering in 2004 and 2006, respectively, from the University of Maryland, College Park, where he is currently pursuing the Ph.D. degree in communication systems.

Since 2006, he has been with U.S. Army RDECOM CERDEC, Fort Monmouth, NJ. His research interests include ultra-wideband communications, cooperative communications, and networking.

Mr. Lai is a Gates Millennium Scholar. He is the recipient of university-level Distinguished Teaching Assistant Award from the University of Maryland.



W. Pam Siritwongpairat (S'03–M'06) received the B.S. degree in electrical engineering from Chulalongkorn University, Bangkok, Thailand, in 1999, and the M.S. and Ph.D. degrees in electrical engineering from the University of Maryland, College Park, in 2001 and 2005, respectively.

She is currently a Wireless Communications Specialist with Meteor Communications Corporation, working on research and development of wireless communications technology. From January 2006 to May 2006, she was a Postdoctoral Research

Associate with the Department of Electrical and Computer Engineering and the Institute for Systems Research (ISR), University of Maryland, College Park. Her research interests span a broad range of areas from signal processing to wireless communications and networking, including space-time coding for multi-antenna communications, cross-layer design for wireless networks, communications in mobile *ad hoc* networks and wireless sensor networks, OFDM systems, and ultra-wideband communications.



K. J. Ray Liu (F'03) received the B.S. degree from National Taiwan University, Taipei, and the Ph.D. degree from the University of California at Los Angeles (UCLA), both in electrical engineering.

He is a Professor and Associate Chair, Graduate Studies and Research, of Electrical and Computer Engineering Department, University of Maryland, College Park. His research contributions encompass broad aspects of wireless communications and networking, information forensics and security, multimedia communications and signal processing,

bioinformatics and biomedical imaging, and signal processing algorithms and architectures.

Dr. Liu is the recipient of numerous honors and awards, including Best Paper awards from the IEEE Signal Processing (SP) Society (twice), the IEEE Vehicular Technology Society, and EURASIP. He was named IEEE SP Society Distinguished Lecturer, and received the EURASIP Meritorious Service Award and National Science Foundation Young Investigator Award. He also received various teaching and research recognitions from the University of Maryland, including a university-level Distinguished Scholar-Teacher Award, Invention of the Year Award, Fellow of Academy for Excellence in Teaching and Learning, and college-level Poole and Kent Company Senior Faculty Teaching awards. He is Vice President—Publications and on the Board of Governor of the IEEE SP Society. He was the Editor-in-Chief of the *IEEE Signal Processing Magazine* and the founding Editor-in-Chief of the *EURASIP Journal on Applied Signal Processing*.